Biosensors and Bioelectronics 129 (2019) 1–6

Contents lists available at ScienceDirect

Biosensors and Bioelectronics

journal homepage: www.elsevier.com/locate/bios

Fabrication of an ultrasensitive and selective electrochemical aptasensor to detect carcinoembryonic antigen by using a new nanocomposite☆

Mohammad Mazloum- Ardakani[a,*], Zahra Tavakolian- Ardakani[a], Nafiseh Sahraei[a], Seyed Mohammad Moshtaghioun[b]

[a] Department of Chemistry, Faculty of Science, Yazd University, Yazd 89195-741, Iran
[b] Department of Biology, Faculty of Science, Yazd University, Yazd 89195-741, Iran

ARTICLE INFO

Keywords:
Aptamer
Carcinoembryonic antigen (CEA)
Electrochemical aptasensor
Hemin
Graphene
Multi-walled carbon nanotube

ABSTRACT

A lable-free electrochemical aptasensor was successfully developed for the sensitive detection of carcinoembryonic antigen as a tumor biomarker. To do this, a ternary nanocomposite of hemin, graphene oxide and multi-walled carbon nanotubes was used. The aptamer can be attached to the surface of a hemin, graphene oxide and multi-walled carbon nanotubes glassy carbon electrode through –NHCO- covalent bonds to form a sensing surface. Through fourier transform infrared spectroscopy and scanning electron microscopy, it was indicated that hemin can be successfully incorporated into hemin, graphene oxide and multi-walled carbon nanotubes. Hemin, which protects graphene nanosheets, also serves as an in-situ probe owing to its well-defined redox properties. Multi-walled carbon nanotubes in the modifier enhance conductivity and facilitate the electron transfer between hemin and the glassy carbon electrode. In this study, carcinoembryonic antigen got specifically bound to the aptamer, and the current changes were used for selective and specific detection of that antigen. The devised aptasensor proved to have excellent performance with a wide linear range of $1.0 \times 10^{-15} - 1.0 \times 10^{-8}$ gmL^{-1} and a detection limit of 0.82 fg mL^{-1}. The inter-day and intra-day values of RSD% were obtained in the range of 0.10–2.91 and 2.21–4.56 respectively. According to the experiments conducted on real samples, it may be claimed that the proposed label-free electrochemical aptasensor is capable enough of determining carcinoembryonic antigen in clinical diagnostics.

1. Introduction

One of the important steps to take for the treatment and control of various types of cancer is the early diagnosis of those diseases. Carcinoembryonic antigen (CEA) is a highly glycosylated cell surface glycoprotein (180 kDa) belonging to a group of substances known as 'tumor-associated antigens' (TAA) (Limbut et al., 2006). The average CEA concentration in a healthy person is under 5 μg L^{-1}, while serum CEA levels higher than 20 μg L^{-1} indicate the presence of cancer (Chauhan et al., 2011; Han et al., 2017) Carcinoembryonic antigen (CEA) is an important tumor marker in the clinical diagnosis of different tumors. For example, over 95% of all colon tumors, 50% of breast tumors, tumors of pancreas, lung, and ovaries as well as some other disorders of the epithelial tissue origin, especially gastrointestinal tract disorders, can be marked or diagnosed by using CEA (Kazuya et al., 1999; M. et al., 1998; Naghibalhossaini and Ebadi, 2006; Prete et al., 2005; Tao et al., 2018; Vogel et al., 2001).

Immunoassays serve as a commonly used method of determining CEA. This method involves the use of different kinds of immunoassay such as colorimetric immunoassay (Zhang et al., 2017, 2013), fluorescent immunoassay (Yan et al., 2012), enzymatic immunoassay (Dela Rosa and Kumakura, 1995), electrochemical immunoassay (Sun et al., 2013), and electrochemiluminescent immunoassay (Zhang et al., 2017, 2013). High specificity and sensitivity are the advantages of immunoassays, but the high cost, low stability and complex operation of antibodies make limitations in their application. Conventional analytical methods used in such analyses are based on chemiluminescence techniques, which provide sensitive and selective detection. Despite

☆ All persons who meet authorship criteria are listed as authors, and all authors certify that they have participated sufficiently in the work to take public responsibility for the content, including participation in the concept, design, analysis, writing, or revision of the manuscript. Furthermore, each author certifies that this material or similar material has not been and will not be submitted to or published in any other publication before its appearance in the journal of Biosensors and Bioelectronics.

* Corresponding author.
E-mail address: mazloum@yazd.ac.ir (M. Mazloum- Ardakani).

https://doi.org/10.1016/j.bios.2018.12.047
Received 18 October 2018; Received in revised form 16 December 2018; Accepted 21 December 2018
Available online 03 January 2019
0956-5663/

these advantages, this technique requires highly skilled technicians for operation and long process. Therefore, there are continuing developments in rapid and cost-effective devices for monitoring including in situ analysis. Electrochemical biosensors are generally powerful analytical tools providing multiplexed analysis, fast response, sensitivity, specificity and low cost. Therefore, new methods with precise, specific and simple operations have been developed to determine CEA in serum. For example, Wang et al. developed a method to determine CEA based on target-induced proximity hybridization coupled with rolling circle amplification (RCA)(Gao et al., 2017). The amount of CEA in this work was determined by the use of an uncharged peptide nucleic acids (PNAs) probe labeled with ferrocene (Fc) as an electroactive indicator on a negatively charged indium tin oxide (ITO) electrode. Also, Zhou et al. (2017) reported a new approach for electrochemical immunoassay based on the hybridization proximity-regulated catalytic DNA hairpin assembly strategy. Among the methods proposed in this regard, one can mention the use of novel biosensors based on aptamers (L, 2007; Liang et al., 2014; Orava et al., 2013; Wang et al., 2015; Wu et al., 2015). Aptamers are artificially fabricated from nucleic acids. They have certain advantages including simple synthesis, good stability, easy chemical modification and extensive applicability in various conditions (Shi et al., 2014).

Hemin is one of the iron porphyrin derivatives which constitutes the active center of hemin-proteins, such as cytochromes, peroxidase, myoglobin, and hemoglobin (Genfa, 1992). It has a reversible redox pair of Fe(III)/Fe(II) and a peroxidase-like activity that is like the activity of the peroxidase enzyme (Zhang et al., 2001). It also possesses a large extinction coefficient in the visible-light region, a predictable rigid structure, and futuristic photochemical electron-transfer capability.

Graphene, as a novel and very promising material for nanocomposites, has attracted a lot of attention in experimental and theoretical scientific communities (Gale et al., 2012). It has a big surface area, great conductivity as well as thermal and potent mechanical strengths (Balandin et al., 2008). Graphene oxide (GO) is one of the important derivatives of graphene. It has a large number of oxygen-functionalized groups on the basal plates and edges, such as carboxyl and epoxide groups (Suk et al., 2010). This makes graphene oxide a good material for combination with other molecules. In recent years, many researchers have used GO for cellular imaging and drug delivery. They have found that, when graphene oxide is used as a carrier, there are many biomolecules attached to it (Sun et al., 2008). Porphyrin was successfully deposited on graphene oxide sheets through a π-π interaction (Xu et al., 2009; Geng and Jung, 2010). Also, hemin-graphene hybrid nanosheets (HGNs) were successfully prepared by a simple wet-chemical strategy (Guo et al., 2011). This nanomaterial has high solubility and stability in water. HGNs have the advantages of both hemin and graphene. They also have an intrinsic peroxidase-like activity ascribed to the presence of hemin.

Multi-walled carbon nanotubes (MWCNTs) include multiple concentric tubes of graphite (Gouveia-Caridade et al., 2008). They have been utilized in biosensors as effective catalyst supports. MWCNTs have attracted remarkable attention due to their fantastic properties such as large surface areas and unique structural and electromechanical properties, high strength and flexibility, high thermal and electrical conductivity, low density, easy preparation, and renewability of their surface (Chauhan et al., 2011; Gouveia-Caridade et al., 2008; Liang et al., 2005; Viswanathan et al., 2009; Ye et al., 2006). These advantages have made MWCNTs appropriate to be used in the preparation of nanotube-reinforced composites.

So far, numerous studies have been carried out to electrochemically determine the ultra-trace amounts of different types of ions, elements and compounds in biological samples and complex matrices (Bojdi et al., 2016, 2014b, 2014a; Hosseini et al., 2014; Kalate Bojdi et al., 2016, 2015b, 2015a).

In this study, we report the use of a novel nanocomposite to modify the surface of a glassy carbon electrode for determination of CEA. The research is in line with the previous studies conducted by our team, including Aghaei et al. (2017), Khoshroo et al. (2018), and Mazloum-Ardakani et al. (2017, 2016b, 2016a, 2015a, 2015c, 2015b). We developed an aptasensor based on a nanocomposite of multi-walled carbon nanotubes, hemin and graphene nanosheets (HGNs-MWCNTs). Accordingly, an easy and inexpensive electrochemical aptasensor was made through assembling CEA binding aptamers (CBA) on the surface of a GCE modified by HGNs-MWCNTs (CBA- HGNs-MWCNTs/GCE). It has already been observed that hemin, with excellent electrochemical activity, if covered on the surface of GNs, can be used as an electrochemical probe for target analysis. Also, the presence of CBA makes the sensing interface bigger, which blocks the electron transfer of hemin and decreases redox signals. When CEA molecules are captured on the interface by CBA, the signals of hemin further decrease due to the thickening of the electron transfers. In this study, in accordance with the variations of the peak currents in the absence and presence of CEA, a label-free electrochemical aptasensor was developed for CEA detection. The results indicate that the proposed sensor is sensitive and specific enough to be used for determination of CEA in clinical diagnoses.

2. Experimental

2.1. Materials and methods

Hemin was obtained from Sigma Chemical Co. Graphite powder and multi-walled carbon nanotube were purchased from Nanostar Co. Ethanolamine (EA), 1-Ethyl-3-(3-dimethy-aminopropyl) carbodiimide hydrochloride (EDC), N-hydroxysuccinimide (NHS), ammonia solution and hydrazine solution were purchased from Merck Co. CEA protein was obtained from Diasorin Co. Following the published protocols, we selected an aptamer with a sequence of: 5′-NH_2-ATACCAGCTTATTCA ATT-5′. The aptamer solution (1 μM) was prepared by a TE buffer (10 mM Tris- HCl, 1 mM EDTA, 0.1 M NaCl, pH = 7.40) and kept at −20 °C before use. Nitric acid, sodium chloride (NaCl), potassium chloride (KOH), urea, glycine, arginine, and glucose were provided from Merck Co. Human serum samples were collected from a local hospital. A phosphate buffer solution (PBS) (0.1 M) with NaOH was used as a supporting electrolyte for electrochemical measurements. Double deionized water was used to prepare aqueous solutions.

2.2. Apparatus

UV–Vis absorption spectra were recorded by an Optizen 3220 UV spectrophotometer. Fourier transform infrared (FTIR) spectroscopy (Perkin Elmer Co.) was done to demonstrate the synthesis of the modifier. All of the electrochemical experiments were performed on an autolab potentiostat/ galvanostat (PGSTAT-302 N, Eco Chemie, Netherlands) in a typical three-electrode system. A modified GCE, a platinum electrode and a saturated calomel electrode (SCE) were used as the working, the counter and the reference electrodes respectively.

2.3. Preparation of the nanocomposite

Firstly, graphene oxide (GO) was produced from graphite powder according to the modified Hummers method (Guo et al., 2011). The HGNs-MWCNTs nanocomposite was synthesized according to the procedure reported in the literature but with a little change in one step. The synthesis was done as follows: 20.0 mL of an aqueous solution containing hemin, graphene oxide and multi-walled carbon nanotube, each for 5 mg mL^{-1}, was sonicated for half an hour. Then, 200.0 μL of an ammonia solution and 30 μL of a hydrazine solution were added to the above solution. The mixture was stirred in a water bath (60 °C) for 3.5 h. For comparison, HGNs were also synthesized with the same method (Guo et al., 2011).

2.4. Preparation of the sensing interface and the electrochemical determination

Before modification, the glassy carbon electrode (GCE) was polished sequentially with 1, 0.3 and 0.05 μm alumina slurry. Then, it was rinsed with deionized water and dried with a stream of N_2 until a mirror-like surface was obtained. Next, 8.0 μL of a 0.5 $mgmL^{-1}$ HGNs-MWCNTs suspension was carefully coated on the GCE surface and dried in air at room temperature to obtain a modified GCE (HGNs-MWCNTs/GCE). Subsequently, the HGNs-MWCNTs/GCE was immersed in a 10 μL phosphate buffer solution (PBS, pH 7.4) containing 0.4 M EDC and 0.2 M NHS to activate the carboxyl-terminated surface for six hours. It was followed by the rinsing of the electrode with PBS (pH 7.4) three times. Then, 5 μL of 1 μM aptamer was coated on the modified GCE surface, and the electrode was put in a humid environment at room temperature for four hours. During this process, the –COOH groups on the interface of the HGNs-MWCNTs nanohybrid were covalently attached by EDC, which then released 1-(3-dimethylamino) propyl-3-ethylurea after reacting with NHS. This structure is suitable for the reaction of aptamers and HGNs-MWCNTs composites through covalent bonds. Briefly, the end –COOH groups were activated with EDC and NHS solutions, and specific aptamers were immobilized on the modified GCE through the formation of amide bonds (Gao et al., 2015; Hu et al., 2018). The electrode was then immersed in 200 μL of 1 mM EA for 15 min to block possible remaining active sites and avoid non-specific adsorption. Thus, a CBA-HGNs-MWCNT aptasensor was obtained.

Eventually, the electrode was incubated in 50 μL of a CEA solution with different concentrations at room temperature for one hour. Then, it was rinsed with PBS to remove the non-specifically bound CEA and dried with N_2. The obtained electrode was in contact with PBS (0.1 M, pH 7.40), and differential pulse voltammetric (DPV) data were obtained in the range of −0.8–0.2 V. The whole process of fabricating the CEA aptasensor and CEA sensing is shown in Scheme 1.

3. Results and discussion

3.1. Characterization of the HGNs-MWCNTs structure

The UV–Vis, FTIR spectra, and FESEM demonstrated the successful synthesis of HGNs-MWCNTs. The morphology of the HGNs-MWCNTs nanocomposite, individual GO, and MWCNTs were determined by FESEM, as shown in Fig. 1. Fig. 1A suggests that GO has a flake-like structure with wrinkles. This structure enhances the surface area. The structures of MWCNTs and HGNs-MWCNTs nanocomposits are observed in Fig. 1B and C respectively. The image of the HGNs-MWCNTs nanocomposite demonstrates that the hemin molecules and MWCNTs are well attached to the graphene sheets. In addition, the hemin molecules are linked to MWCNTs too. This 3D nanohybrid increased the surface area and the electron transfer.

The UV–Vis spectrum is presented in Fig. S1 in the "supplementary materials" file. The GO dispersion (curve a) displays a strong absorption at approximately 225 nm corresponding to the π– π * transition of the aromatic C=C bands and a shoulder at 290–310 nm which is related to the n–π^* transition of the C=O bands. The spectra of the hemin solution (curve b) exhibit a maximum absorption at about 390 nm and a series of weak peaks at about 600 nm, which are due to the Soret band and the Q-bands of hemin respectively (Coliman et al., 1975). For HGNs (curve c), the absorption curve is characterized by a strong absorption band at ~ 265 nm, which is attributed to the reduced GO (RGO), and another peak at ~ 415 nm with a bathochromic shift, which corresponds to the Soret band of hemin. This band clearly shows a π–π stacking interaction between the porphyrin ring and RGO.

In addition, the red shift of the absorption peak of the GO dispersal (225–265 nm) can be due to the electronic conjugation in GNs that is repaired by the reduction of hydrazine. In the case of the absorption spectrum of HGNs-MWCNTs (curve d), one can see all the characteristics of the absorption band in the previous spectrum. Also, the

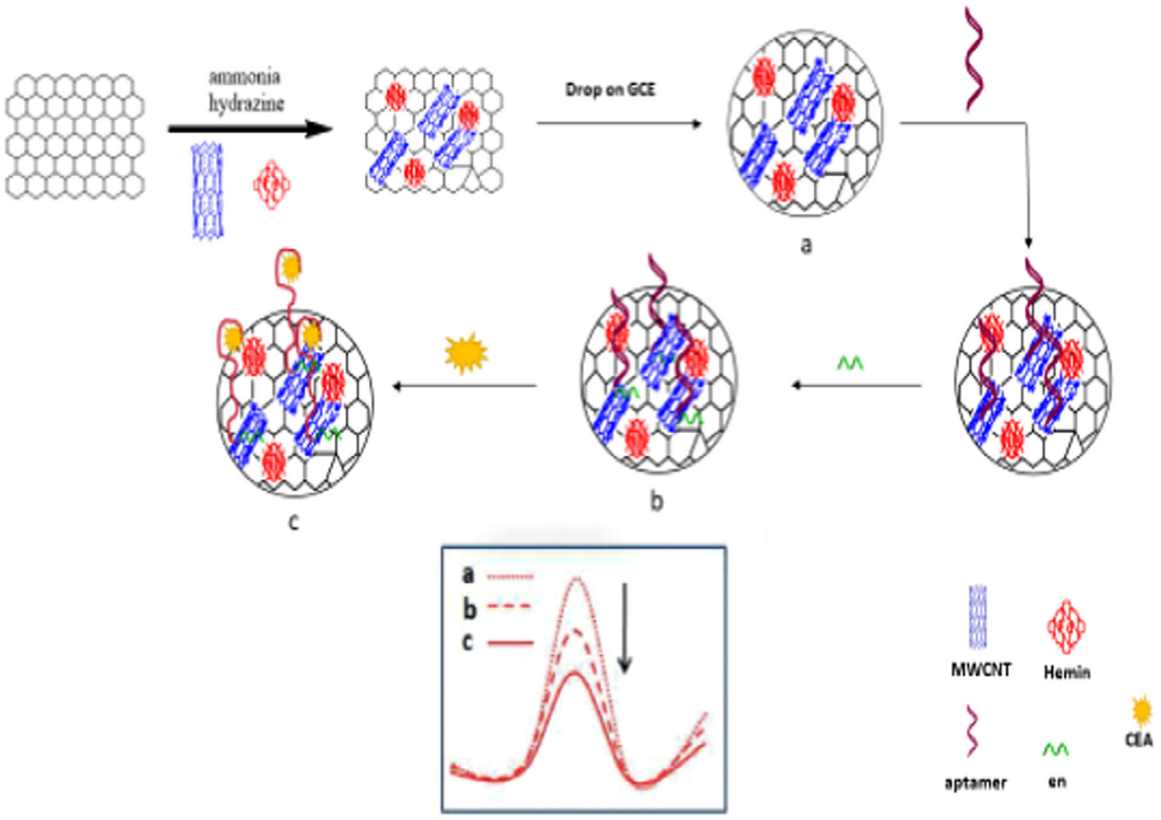

Scheme 1. Schematic illustration of the preparation and working of the aptasensor proposed for CEA detection.

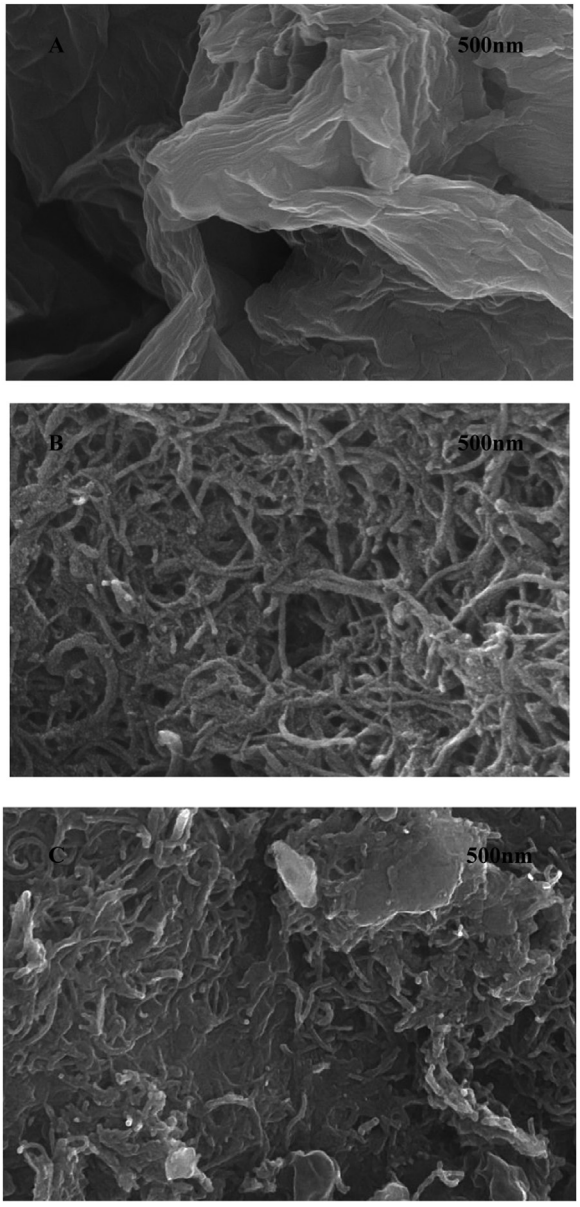

Fig. 1. FE-SEM image of (A) the GO layer, (B) the MWCNTs layer, and (C) the HGNs-MWCNTs nanocomposite layer on the GCE.

absorption peak of 415 nm is stronger, which indicates hemin could successfully combine with GNs and MWCNTs through the π—π interaction.

The FTIR spectrum can confirm useful information about the structure of the HGNs-MWCNTs nanocomposite. Fig. S2 exhibits the comparative FTIR spectra of hemin, GO, MWCNT and HGNs-MWCNTs. Curve a shows the characteristic absorption of hemin. The band at 1710 cm $^{-1}$ is attributed to the C=O stretch mode of the carboxylic group, and the bands at 1407 cm^{-1} and 1453 cm^{-1} are assigned to the contribution of the C-H bending vibration. The absorption bands between 1000 and 3000 cm^{-1} are attributed to the C-O stretching vibration in the aromatic ring of hemin and the =C-H bending vibration of olefin at 844 cm^{-1}. These findings are consistent with other reports in the literature, such as Zhang et al. (2005) and Zhu et al. (2016). The FTIR spectra of GO (curve b) indicates a broad absorption band at 3440 cm^{-1} which is attributed to the OH groups. Also, the appearance of the absorption bands at 1646 cm^{-1} and 1759 cm^{-1} indicates the existence of carbonyl stretching vibration; carbonyl and carboxyl groups are bound to the edges of the planes of GO (Zhang et al., 2010).

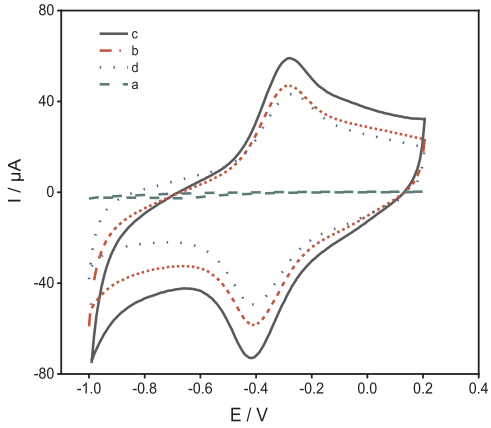

Fig. 2. Cyclic voltammograms of the modified electrode after the assembling steps of the aptasensor preparation: (a) bare GCE, (b) HGNs/ GCE, (c) HGNs-MWCNTs/ GCE and (d) CBA- HGNs-MWCNTs/ GCE in 0.1 M PBS (pH 7.4). Scan rate: 100 mV s^{-1}.

The obvious absorption peaks at 2330, 1630 and 1257 cm^{-1} indicate the existence of carboxylic and carboxylate oxygen groups on the MWCNTs surface (curve c). In comparison, the FTIR spectra of HGNs-MWCNTs show the representative absorption bands of hemin besides the absorption peaks of GO and MWCNs (curve d). These results confirm the successful formation of the HGNs-MWCNTs nanocomposite. Fig. S3 shows the BET of the electrode material and specific area of electrode was 29.99 m^2.g^{-1}.

3.2. Electrochemical behavior of the modified electrode (CBA-HGNs-MWCNTs/GCE)

Cyclic voltammetry (CV) and differential pulse voltammetry (DPV) techniques were used to investigate the electrochemical behavior of the CBA-HGNs-MWCNTs/GCE. Fig. 2 displays the CVs of the bare GCE (curve a), the HGNs/GCE (curve b), the HGNs-MWCNTs/GCE (curve c), and the CBA-HGNs-MWCNTs/GCE (curve d) in a 0.1 M PBS buffer solution. As the figure suggests, the bare GCE presents no observable peak, but the HGNs-modified electrode displays a pair of well-defined redox peaks in the potential range. This can be attributed to the characteristics of the single-electron transfer process of the Fe (III)/Fe (II) redox couple in the core of hemin. As expected, the HGNs-MWCNTs-modified electrode exhibited a pair of higher redox peak currents of hemin, which can be due to the presence of MWCNTs in the modifier. This facilitated the electron transfer between hemin and the GCE. Cyclic voltammograms of the HGNs-MWCNTs/GCE were taken at various scan rates and displayed in Fig. S4. As it can be seen, the redox peak currents vary linearly once the scan rate increases. This implies that embedding of hemin in the modifier is a surface-controlled process.

3.3. Effect of CEA incubation time

To be sensed by the modified electrode, CEA had to be specifically bonded to CBA on the surface of the CBA-HGNs-MWCNTs/GCE. Therefore, the effect of the incubation time of 1 ng mL^{-1} CEA on the response of the aptasensor was studied. The DPV peak current decreased rapidly with an increase in the incubation time due to the increased CEA on the surface of the aptasensor. After 60 min, the plot became almost flat, representing the surface saturation. Hence, this time was selected to be the optimum incubation time. The curve for the optimization of the incubation time is provided in Fig. S5.

3.4. CEA detection

Under the above optimal experimental conditions, the quantitative

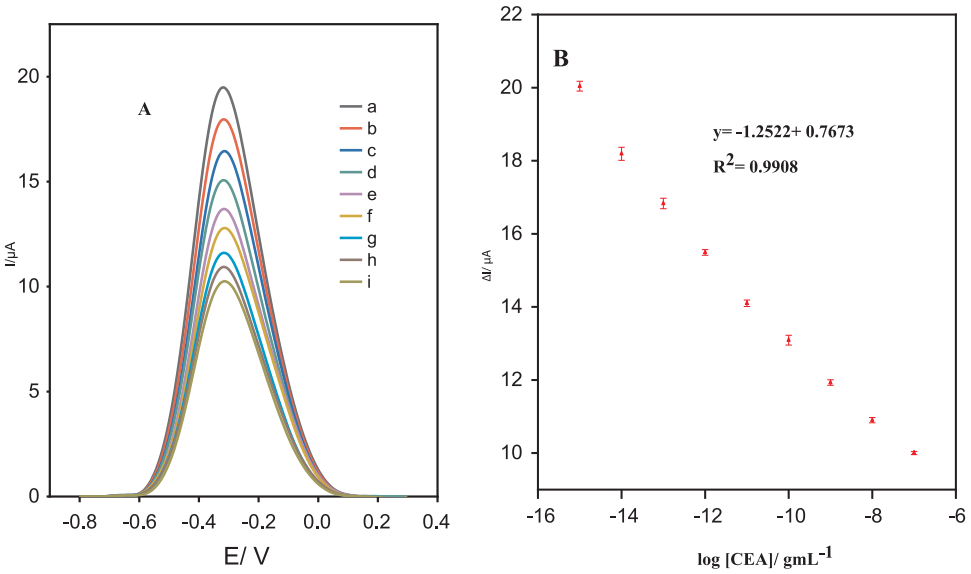

Fig. 3. (A) DPV analysis for different concentration of CEA (a) 1.0×10^{-15} (b) 1.0×10^{-14} (c) 1.0×10^{-13} (d) 1.0×10^{-12} (e) 1.0×10^{-11} (f) 1.0×10^{-10} (g) 1.0×10^{-9} (h) 1.0×10^{-8} and (i) 1.0×10^{-7} gmL^{-1} at the aptasensor in 0.1 M PBS (pH 7.4). (B) Calibration curve for ΔI vs. log [C_{CEA}] (gmL^{-1}).

Table 1
Brief specifications of the previously reported CEA aptasensor.

Methods	Linear range	Detection limit	References
Capillary electrophoresis-chemiluminescence	0.0654–6.54 ng/mL	8 pg/mL	(Zhou et al., 2015)
Electrochemical aptasensor	0.0001–10 ng/mL	40 fg/mL	(Liu et al., 2016)
Electrochemical immunosensor	0.1–750.0 ng/mL	90 pg/mL	(Liu et al., 2015)
Electrochemical immunosensor	10–12 × 10^5 pg/mL	8 pg/mL	(Huang et al., 2015)
Electrochemical aptasensor	1.0 fg/mL- 10 ng/mL	0.68 fg/mL	This work

determination of CEA by means of the aptasensor was performed using DPV. As presented in Fig. 3, the decreased peak current (Δi) was just proportional to the logarithmic concentration of CEA in the range of 1.0×10^{-15} – 1.0×10^{-8} gm L^{-1} (R^2 = 0.9906), with the method detection limit of 0.82 fg/mL based on signals-to-noise ratio (3 S/N). Compared with most of the sensors previously developed for CEA detection, as summarized in Table 1, this aptasensor exhibited an excellent detection limit and linear range. The results showed that, in some cases, the aptasensor proposed in this study had better detection limits and, in other cases, it had a better linear range than the previous ones. In addition, the construction of this biosensor was less costly than the other ones.

It was indicated that the ternary nanocomposite of hemin, graphene and multi-walled carbon nanotubes can successfully serve as a modifier for detection of CEA with the aptamer developed here. This is due to a set of excellent properties of GN, hemin and MWCNTs. These properties are as follows:

1) Improvement of the performance of the modified electrode due to the excellent conductivity of the ternary nanohybrid of HGNs-MWCNTs as well as the synergistic effect of these three well-combined materials
2) Increase of the surface area of the electrode due to the combination of 1D MWCNTs with 2D GN and the formation of a 3D nanohybrid
3) Attachment of hermin to the surface of the modified electrode which provides a good interface for connection of the aptamer to the surface electrode
4) Significant reduction of the aggregation and stacking among the three materials by the formed nanohybrid through creating a space between them, as also reported by Kong et al. (2015)

3.5. Specificity, repeatability and stability of the aptasensor

The selectivity of the aptasensor plays an important role in analyzing real samples. Evaluation of the specificity of this aptasensor was done by detecting the DPV current changes in a 1.0 ngmL^{-1} CEA solution containing 500 ng mL^{-1} of different possibly coexisting interferences in human serum, such as insulin (INS), urea, glucose, arginine, glycine and human serum albumin (HAS). The current variation due to the interferences was less than about 3% of that without the interfering substances except insulin. For insulin, the amount of variation was 5.2%. These results indicated that the aptasensor could detect CEA very selectively (Fig. S6). In addition, the repeatability of the aptasensor was investigated by detecting a 1.0 ng mL^{-1} CEA solution through five replicate experiments. The relative standard deviation (RSD) was 7.6%, which points to a proper repeatability. The stability of the proposed aptasensor was also evaluated periodically by detecting its DPV current responses. The aptasensor was stored in a container kept in a refrigerator at 4 °C. It was tested on a daily basis in a period of two weeks. After this time, 92% of the initial peak current remained, which is indicative of the acceptable stability of the aptasensor.

3.6. Real sample analysis

In order to evaluate the practical application of the proposed aptasensor in detection of CEA in biological samples, the standard addition method was applied. For this purpose, 30 μL of human serum was diluted to 3.0 mL with PBS, and then different amounts of CEA were added to 1 mL of the diluted samples. Table 2 shows the analytical results and the recoveries. The recoveries of the spiked samples varied in the range of 95.00–103.00%. The inter-day and intra-day values of RSD% were obtained in the range of 0.10–2.91 and 2.21–4.56 respectively. The range of recovery suggests the proposed aptasensor can be

Table 2
Recovery results of the aptasensor for CEA detection.

Samples	Added ($ngmL^{-1}$)	Found ($ngmL^{-1}$)	Recovery (%)	RSD (%) inter- day	RSD (%) intra- day
1	0.01	9.68×10^{-3}(± 0.01)	96.80	0.10	2.21
2	0.10	1.03×10^{-1}(± 0.03)	103.00	2.91	4.56
3	1.00	9.50×10^{-1}(± 0.02)	95.00	0.21	2.42

used to determine CEA in real samples with good accuracy.

4. Conclusions

In this study, a facile label-free electrochemical aptasensor was developed for detection of CEA. The aptasensor was fabricated based on a ternary nanocomposite of HGNs-MWCNTs. This modifier can provide an integrated set of the main excellent properties of graphene oxide, hemin, and MWCNTs. Fabrication of electrochemical aptasensors with aminated aptamers can limit the use of the Au modification technique and decrease production costs due to employing inexpensive modifying materials such as graphene oxide or MWCNTs. In optimum conditions, the electrochemical aptasensor detected CEA in a concentration range from 1.0×10^{-15} g mL^{-1} to 1.0×10^{-8} gmL^{-1}, with a method detection limit of 0.82 fg mL^{-1}. The aptasensor for CEA detection demonstrated high selectivity, good reproducibility and acceptable stability. We, thus, propose the use of this low-cost and highly sensitive and selective CEA aptasensor as a promising approach for determination of CEA in biological and clinical applications.

Acknowledgements

The authors wish to thank the Iran National Science Foundation (INSF), Yazd University Research Council and IUT Research Council and Excellence in Sensors for financial support of this research.

Declaration of interests

None

Appendix A. Supporting information

Supplementary data associated with this article can be found in the online version at doi:10.1016/j.bios.2018.12.047.

References

Aghaei, R., Mazloum-Ardakani, M., Abdollahi-Alibeik, M., Moshtaghioun, S.M., Rezaeipoor-Anari, A., Haghighijoo, Z., Zamani, L., 2017. J. Electroanal. Chem. 796, 24–32.
Balandin, A.A., Ghosh, S., Bao, W., Calizo, I., 2008. Superior thermal conductivity of single-layer graphene. Nano Lett. 8, 902–907.
Bojdi, M.K., Behbahani, M., Hesam, G., Mashhadizadeh, M.H., 2016. RSC Adv. 6, 32374–32380.
Bojdi, M.K., Behbahani, M., Sahragard, A., Amin, B.G., Fakhari, A., Bagheri, A., 2014a. Electrochim. Acta 149, 108–116.
Bojdi, M.K., Mashhadizadeh, M.H., Behbahani, M., Farahani, A., Davarani, S.S.H., Bagheri, A., 2014b. Electrochim. Acta 136, 59–65.
Chauhan, N., Narang, J., Pundir, C.S., 2011. Analyst 136, 1938.
Coliman, J.P., Gagne, R.R., Reed, C.A., Halbert, T.R., Robinson, W.T., Lang, G., 1975. J. Am. Chem. Soc. 97, 1427–1439.
Dela Rosa, A.M., Kumakura, M., 1995. Anal. Chim. Acta 312, 85–94.
Gale, J.D., Geim, A.K., Novoselov, K.S., Castro Neto, A.H., Peres, N.M.R., Novoselov, K.S., Geim, A.K., Tuckerman, M.E., Tomadin, A., Loya, A., Stair, J.L., Ren, G., Geim, A.K., Novoselov, K.S., Geim, A.K., Novoselov, K.S., Dewapriya, M.A.N., Barker, J. a., Henderson, D., Anderson, T.L., Ariza, M.P., Ortiz, M., Wang, M.C., Yan, C., Ma, L., Hu, N., Chen, M.W., Carpio, A., Bonilla, L.L., De Juan, F., Vozmediano, M.A.H., 2012. Rev. Mod. Phys. 58, 710–734.
Gao, F., Zhou, F., Chen, S., Yao, Y., Wu, J., Yin, D., Geng, D., Wang, P., 2017. Analyst 142, 4308–4316.
Gao, L., Xiao, Y., Wang, Y., Chen, X., Zhou, B., Yang, X., 2015. Talanta 132, 215–221.
Genfa, Z., Dasgupta, Purnendu K., 1992. Anal. Chem. 64, 517–522.
Geng, J., Jung, H., 2010. Nano 8227–8234.
Gouveia-Caridade, C., Pauliukaite, R., Brett, C.M.A., 2008. Electrochim. Acta 53, 6732–6739.
Guo, Y., Deng, L., Li, J., Guo, S., Wang, E., Dong, S., 2011. ACS Nano 5, 1282–1290.
Han, J., Li, Y., Feng, J., Li, M., Wang, P., Chen, Z., Dong, Y., 2017. J. Electroanal. Chem. 786, 112–119.
Hosseini, H., Behbahani, M., Mahyari, M., Kazerooni, H., Bagheri, A., Shaabani, A., 2014. Biosens. Bioelectron. 59, 412–417.
Hu, X., Goud, K.Y., Kumar, V.S., Catanante, G., Li, Z., Zhu, Z., Marty, J.L., 2018. Sens. Actuators B: Chem. 268, 278–286.
Huang, J., Tian, J., Zhao, Y., Zhao, S., 2015. Sens. Actuators B: Chem. 206, 570–576.
Kalate Bojdi, M., Behbahani, M., Mashhadizadeh, M.H., Bagheri, A., Hosseiny Davarani, S.S., Farahani, A., 2015a. Mater. Sci. Eng. C 48, 213–219.
Kalate Bojdi, M., Behbahani, M., Najafi, M., Bagheri, A., Omidi, F., Salimi, S., 2015b. Electroanalysis 27, 2458–2467.
Kalate Bojdi, M., Behbahani, M., Omidi, F., Hesam, G., 2016. New J. Chem. 40, 4519–4527.
Khoshroo, A., Mazloum-Ardakani, M., Forat-Yazdi, M., 2018. Sens. Actuators B: Chem. 255, 580–587.
Kong, F.Y., Li, W.W., Wang, J.Y., Fang, H.L., Fan, D.H., Wang, W., 2015. Anal. Chim. Acta 884, 37–43.
Kazuya, Kudoh, Tsunekazu, Kita, Takehiko, Tode, Masashi, Takano, Junko, Hirata, Yoshinori, Mano, Kenji, Yamamoto, Ichiro, Nagata, Y, K., 1999. Obstet. Investig. 47, 52–57.
L, W., 2007. J. Nanjing Med. Univ. 21, 277–281.
Liang, K., Zhai, S., Zhang, Z., Fu, X., Shao, J., Lin, Z., Qiu, B., Chen, G.N., 2014. Analyst 139, 4330–4334.
Liang, Y., Zhang, H., Yi, B., Zhang, Z., Tan, Z., 2005. Carbon N. Y. 43, 3144–3152.
Limbut, W., Kanatharana, P., Mattiasson, B., Asawatreratanakul, P., Thavarungkul, P., 2006. Anal. Chim. Acta 561, 55–61.
Liu, J., Wang, J., Wang, T., Li, D., Xi, F., Wang, J., Wang, E., 2015. Biosens. Bioelectron. 65, 281–286.
Liu, Z., Wang, Y., Guo, Y., Dong, C., 2016. Electroanalysis 28, 1023–1028.
M, T., Y, T., Y, N., S, K., T, K., D.K, D., H, K., 1998. J. Am. Coll. Surg. 187, 64–68.
Mazloum-Ardakani, M., Aghaei, R., Abdollahi-Alibeik, M., Moaddeli, A., 2015a. J. Electroanal. Chem. 738, 113–122.
Mazloum-Ardakani, M., Ahmadi, S.H., Safaei Mahmoudabadi, Z., Khoshroo, A., 2016a. J. Int. Meas. Confed. 91, 162–167.
Mazloum-Ardakani, M., Dehghani-Firouzabadi, A., Sheikh-Mohseni, M.A., Benvidi, A., Mirjalili, B.B.F., Zare, R., 2015b. J. Int. Meas. Confed. 62, 88–96.
Mazloum-Ardakani, M., Farbod, F., Hosseinzadeh, L., 2016b. J. Nanostruct. 6, 293–300.
Mazloum-Ardakani, M., Khoshroo, A., Hosseinzadeh, L., 2015c. Sens. Actuators B: Chem. 214, 132–137.
Mazloum-Ardakani, M., Maleki, M., Khoshroo, A., 2017. J. Iran. Chem. Soc. 14, 1659–1664.
Naghibalhossaini, F., Ebadi, P., 2006. Cancer Lett. 234, 158–167.
Orava, E.W., Abdul-Wahid, A., Huang, E.H.B., Mallick, A.I., Gariépy, J., 2013. Mol. Oncol. 7, 799–811.
Prete, S.P., Rossi, L., Correale, P.P., Turriziani, M., Baier, S., Tamburrelli, G., De Vecchis, L., Bonmassar, E., Aquino, A., 2005. Pharmacol. Res. 52, 167–173.
Shi, G.F., Cao, J.T., Zhang, J.J., Huang, K.J., Liu, Y.M., Chen, Y.H., Ren, S.W., 2014. Analyst 139, 5827–5834.
Suk, J.W., Piner, R.D., An, J., Ruoff, R.S., 2010. ACS Nano 4, 6557–6564.
Sun, G., Lu, J., Ge, S., Song, X., Yu, J., Yan, M., Huang, J., 2013. Anal. Chim. Acta 775, 85–92.
Sun, X., Liu, Z., Welsher, K., Robinson, J.T., Goodwin, A., Zaric, S., Dai, H., 2008. Nano Res. 1, 203–212.
Tao, Z., Du, J., Cheng, Y., Li, Q., 2018. Int. J. Electrochem. Sci. 13, 1413–1422.
Viswanathan, S., Rani, C., Vijay Anand, A., Ho, J. an A., 2009. Biosens. Bioelectron. 24, 1984–1989.
Vogel, I., Francksen, H., Soeth, E., Henne-Bruns, D., Kremer, B., Juhl, H., 2001. Am. J. Surg. 181, 188–193.
Wang, D., Li, Y., Lin, Z., Qiu, B., Guo, L., 2015. Anal. Chem. 87, 5966–5972.
Wu, Z.J., Li, H., Liu, Z.H., 2015. Sens. Actuators B: Chem. 206, 531–537.
Xu, Y., Liu, Z., Zhang, X., Wang, Y., Tian, J., Huang, Y., Ma, Y., Zhang, X., Chen, Y., 2009. Adv. Mater. 21, 1275–1279.
Yan, M., Ge, S., Gao, W., Chu, C., Yu, J., Song, X., 2012. Analyst 137, 2834–2839.
Ye, J.S., Cui, H.F., Wen, Y., Zhang, W., De, Xu, G.Q., Sheu, F.S., 2006. Microchim. Acta 152, 267–275.
Zhang, A., Huang, C., Shi, H., Guo, W., Zhang, X., Xiang, H., Jia, T., Miao, F., Jia, N., 2017. Sens. Actuators B Chem. 238, 24–31.
Zhang, C., Ren, L., Wang, X., Liu, T., 2010. J. Phys. Chem. C 114, 11435–11440.
Zhang, X., Zhang, Y., Jiang, J., 2005. Spectrochim. Acta - Part A Mol. Biomol. Spectrosc. 61, 2576–2583.
Zhang, Y., Liu, W., Ge, S., Yan, M., Wang, S., Yu, J., Li, N., Song, X., 2013. Biosens. Bioelectron. 41, 684–690.
Zhang, Y., Zhang, C., Shen, eH., 2001. Electroanalysis 13, 1431–1435.
Zhou, F., Yao, Y., Luo, J., Zhang, X., Zhang, Y., Yin, D., Gao, F., Wang, P., 2017. Anal. Chim. Acta 969, 8–17.
Zhou, Z.M., Feng, Z., Zhou, J., Fang, B.Y., Ma, Z.Y., Liu, B., Zhao, Y., Di, Hu, Bin, X., 2015. Sens. Actuators B: Chem. 210, 158–164.
Zhu, Y., Yan, K., Xu, Z., Zhang, J., 2016. J. Electrochem. Soc. 163, B526–B532.